文章编号 2095-1531(2018)02-0190-08

High-speed 850 nm vertical-cavity surface-emitting lasers with BCB planarization technique

HE Xiao-ying[1], DONG Jian [2], HU Shuai[2], HE Yan [2], LV Ben-shun[2],
LUAN Xin-xin[2], LI Chong[2], HU Zong-hai[1], GUO Xia[1*]
(1. *School of Electronic Engineering, State Key Laboratory of Information Photonics and Optical Communications, Beijing University of Posts and Telecommunications, Beijing* 100876, *China*;
2. *School of Information, Beijing University of Technology, Beijing* 100124, *China*)
* *Corresponding author, E-mail: guox@ bupt. edu. cn*

Abstract: Vertical-cavity surface-emitting lasers(VCSELs) are widely used in short-reached optical interconnects and data communication links because of their low energy consumption and high modulation speed. Capacitance, as the parasitic parameters, affects the modulation bandwidth. In this paper, parasitic capacitance of VCSELs is reduced by using a low-*k* benzocyclobutene(BCB) planarization technique. The detail BCB planarization technique has been discussed with optimal process parameters, which is useful for high-speed VCSEL fabrication. The small signal modulation bandwidth of the low-*k* BCB planarization VCSEL with 7 μm oxide aperture has been achieved to 15. 2 GHz.

Key words: vertical-cavity surface-emitting laser; high-speed modulation; benzocyclobutene(BCB) planarization technique

采用 BCB 平整技术的高速 850 nm 垂直面发射激光器

何晓颖[1],董 建[2],胡 帅[2],何 艳[2],吕本顺[2],
栾信信[2],李 冲[2],胡安琪[1],胡宗海[1],郭 霞[1*]
(1. 北京邮电大学 电子工程学院,信息光子学与光通信国家重点实验室,北京 100876;
2. 北京工业大学 信息学部,北京 100124)

摘要:垂直腔面发射激光器因其具有低阈值、低功耗、可实现高速调制等优势,广泛地应用于光通信和光互连等领域。寄生电容是影响激光器的调制带宽的主要因素之一。本文通过采用低 *k* 值的苯并环丁烯(BCB)平整技术有效地降低了垂

收稿日期:2017-11-17;**修订日期**:2017-12-16
基金项目:国家自然科学基金资助项目(No. 61335004, No. 61675046, No. 61505003);国家重大研发计划(No. 2016YFB0400603, No. 2017YFB0400902, No. 2017YFF0104801)
Supported by National Natural Science Foundation of China(No. 61335004, No. 61675046, No. 61505003); National Key R&D Program of China(No. 2016YFB0400603, No. 2017YFB0400902, No. 2017YFF0104801)

直腔面发射激光器的寄生电容。详细研究了 BCB 平整技术的最优工艺参数,为未来高速垂直腔面发射激光器的制造技术提供参考。低 k 值 BCB 平整垂直腔面发射激光器在 7 μm 氧化孔径下 3 dB 小信号调制带宽可达 15.2 GHz。

关　键　词:垂直腔面发射激光器;高速调制;苯并环丁烯平整技术

中图分类号:TN248.4　　**文献标识码**:A　　doi:10.3788/CO.20181102.0190

1　Introduction

850 nm vertical-cavity surface-emitting lasers (VCSELs) are standard light sources for short-reached optical interconnects and data-communication links, including supercomputer clusters and data centers, because of their high modulation speed, low power consumption, low current operation, good beam quality, and *etc.*[1-3]. The modulation frequency of the VCSELs is mainly limited by their intrinsic resonance frequency, damping, and extrinsic parasitic parameters. Many methods were proposed to improve the modulation frequency of VCSELs, such as applying InGaAs/AlGaAs strain quantum wells to increase the differential gain and then the modulation frequency[4], optimizing the photon lifetime through etching top distributed Bragg reflector (DBR) to reduce the damping[5-6], and growing multiple oxide layers to decrease the oxide capacitance which is the largest parasitic capacitance in the devices[7-9].

In order to decrease the oxide capacitance, Benzocyclobutene (BCB), which is an important material for high-speed devices, is introduced into the VCSELs. Because it has a low dielectric constant of 2.65, lower to other frequently-used dielectric materials including SiO_2 and polyimide with dielectric constant of 3.9 and 3.3, respectively[10]. By planarizing the low-k BCB film between the P- and the N-type ohmic contact layer, the pad capacitance can be greatly reduced due to the capacitance calculation equation[11-12].

In this paper, high-speed oxide-confined 850 nm GaAs quantum wells (QWs) VCSELs using a low-k BCB planarization technique to reduce parasitic capacitance are reported. The small signal modulation bandwidths of the VCSEL with oxide aperture of 5 μm and 7 μm are demonstrated.

2　Design and Fabrication of High Speed VCSEL

The epitaxial structure of the VCSEL was grown by metal-organic chemical vapor deposition on a (100)-oriented n^+-GaAs substrate. A graded separate confinement heterostructure region containing an active region with 3 unstrained 7 nm thick GaAs multiple quantum wells (MQWs) separated by 8 nm thick $Al_{0.3}Ga_{0.7}As$ barriers was centered in the one-λ resonant optical cavity with p-type and n-type $Al_{0.3}Ga_{0.7}As$ phase compensation layers. The photoluminescence peak was located at 835 nm. 20.5 pairs of p-doped and 35 pairs of n-doped graded $Al_{0.90}Ga_{0.10}As/Al_{0.12}Ga_{0.88}As$ DBRs were located on each side of the active region, respectively. A 30 nm thick $Al_{0.98}Ga_{0.02}As$ layer, which was located near a node in the cavity standing wave profile where the optical intra-cavity scattering loss was reduced, was included in the top DBR to allow for selective oxidation during fabrication and then for transverse optical and electrical confinement. The topmost DBR layer consists of a 25 nm thick heavily p^+-doped GaAs layer, located on top of the p-type DBR as a low-contact resistance layer.

Both the top and bottom mesa were fabricated by wet etching. The oxide aperture was formed in a wet oxidation furnace at 390 ℃ with an N_2 flow of 1 L/min, giving an oxidation rate of approximately 0.52 μm/min for the $Al_{0.98}Ga_{0.02}As$ layers. An oxide aperture of 7 μm was selected. Ti/Au was sputtered on the top surface to form the ohmic contacts. Then, the devices were annealed in a rapid thermal

annealing system at 430 ℃ in an N_2 atmosphere. Coplanar ground-signal-ground (GSG) contacts were applied for direct high-frequency probing measurements, in order to avoid parasitic coupling at the probe tips and thus improve the measurement accuracy of the microwave probing test[13].

In this paper, the BCB is used to decrease the oxide capacitance of the VCSEL. Fig. 1(a) shows the simulation results of the small signal modulation performance for the VCSELs with SiO_2 and BCB passivation, which comes from the small signal modulation transfer function derived by carrier and photon kinetic equations[14]. The parasitic cutoff frequency for VCSELs with the BCB passivation can reach to ~17.8 GHz, higher than that for SiO_2-passivated ones about 10.6 GHz. Fig. 1(b) demonstrated the small signal modulation response results measured by network analyzer, where the VCSELs are respectively passiated by SiO_2 and BCB both with the oxide aperture of 7 μm@6 mA. The −3 dB small signal modulation bandwidth is 15.2 GHz and 9.85 GHz, respectively, which indicates the modulation bandwidth limits by the RC parasitic parameter, thus to greatly increase its cutoff frequency depending on BCB passivation.

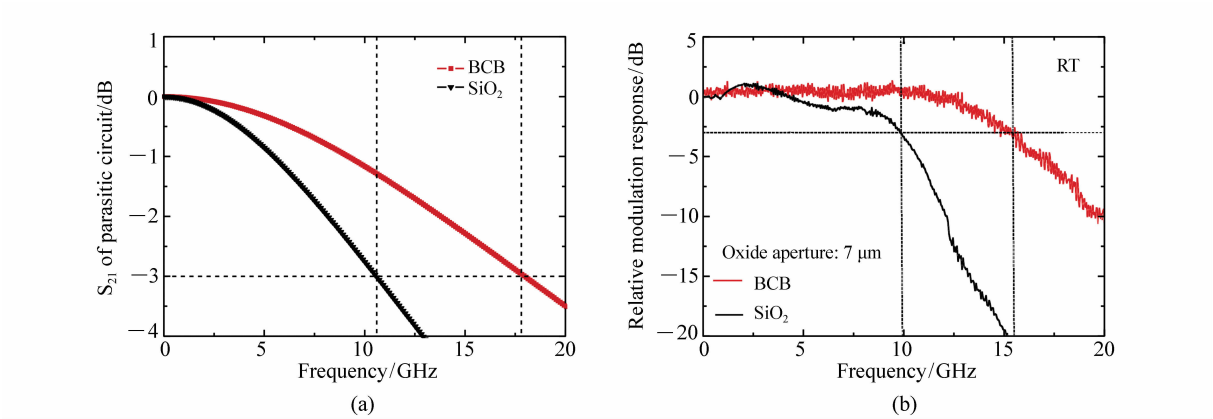

Fig. 1 (a) Simulation results of small signal modulation response for VCSELs with BCB and SiO_2 passivation. The parasitic cutoff frequency can reach to 17.8 GHz and 10.6 GHz for BCB and SiO_2-passivated VCSEL, respectively. (b) The measured small signal modulation response for VCSELs with BCB and SiO_2 passivation. The −3dB bandwidth is 15.2 GHz and 9.85 GHz with the oxide aperture of 7 μm@6 mA, respectively, which indicates the parasitic capacitance limits the modulation frequency of the devices

The schematic cross-sectional structure of high speed VCSEL devices is shown in Fig. 2(a).

The photosensitive BCB is coated on the VCSEL surface by spinning process. Fig. 3(a) presents the dependence of the spinning speed on the BCB thickness before and after hard baking of 1.5 min with the temperature of 70 ℃ in the oven. According to the epitaxial structure, the spinning speed is selected to be 2 000 r/min with the BCB thickness of around 6 μm. The thick film requires more exposure energy. Fig. 3(b) shows the relationship of exposure time with the diameter difference (Δd) between patterns on the mask and on the devices. Fig. 2(b) presents a top-view image of the high-speed VCSEL.

Generally, the pattern size on the devices is larger than that on the mask. The diameter difference increases with the exposure time because the diffraction occurs at the edge of the mask patterns. Decreasing the exposure time will decrease the pattern size discrepancy, however, and the residues on the patterns are hard to be removed due to the thick BCB film determined by the VCSEL structure. Fig. 3(c) demonstrates the microscopic image of the exposed area. Colorful strips are caused by the refractive index difference between the residue BCB and the sub-

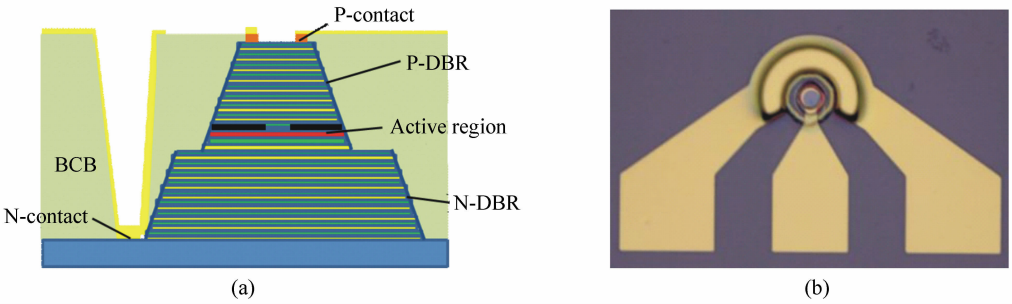

Fig. 2　(a) Schematic cross-sectional structure of high-speed VCSEL devices. (b) Top-view image of the high-speed VCSEL with coplanar GSG electrode structure

strate, which will deteriorate the Ohmic contact. In our experiment, inductively coupled plasma (ICP) etching with SF_6 and O_2 chemistry is applied to remove these BCB residues. Fig. 3(d) demonstrates the microscopic image of the pattern after the ICP etching using SF_6/O_2 chemistry with ICP power of 1 000 W and RF power of 50 W.

3　Static and Dynamic Performance Characteristics

The static light output power-current-voltage (L-I-V) characteristics were measured under the wafer probes at room temperature. The L-I-V results for BCB planarization VCSELs with the 5 μm and 7 μm oxide aperture diameter are shown in Fig. 4(a). It can be seen that the threshold currents I_{th} are 0.12 mA and 0.22 mA, and the threshold electrical powers are 0.65 mW and 0.84 mW at the 5 μm and 7 μm oxide aperture, respectively[15], while the threshold current density J_{th} is about 0.57 kA/cm^2. As the current injection increases, the photon density in the active region increases and the optical power also increases. Correspondingly, the maximum output optical power increased with aperture size. The maximum output optical power reached to 0.47 mW at a 9 mA and 0.68 mW at a 12 mA respectively for the 5 μm and 7 μm oxide aperture VCSELs. That is because red shift in wavelength and decrease in efficiency would be caused by self-heating effects, and optical power therefore decreased rapidly. The differential resistance, depending on the size of the oxide aperture and epitaxial structure[16], are 212 Ω and 190 Ω at the 5 μm and 7 μm oxide aperture, which determines the thermal roll-over current of the VCSELs.

The small signal modulation response of the VCSELs was measured using a 40 GHz R&S ZVA 40 network analyzer and a high-frequency microwave probe (Picoprobe 40A-GSG-150-P) to contact the device under test. A multimode fiber was connected to a 25 GHz high-speed photodetector (New Focus 1414-50), and the signal after detection was connected back to the network analyzer with a high-frequency cable. Before testing the VCSELs, calibrations were made to compensate for losses caused by the cables and the probe insertion[17]. Fig. 5 show small-signal modulation response at room temperature at different bias currents for the 5 μm(a) and 7 μm(b) oxide aperture VCSELs with BCB planarization. For the 5 μm oxide aperture VCSEL, as the injection current increases from 2 mA to 5 mA, the small signal modulation bandwidth increases from 12.8 GHz to the maximum 15 GHz due to increased gain. Then the modulation bandwidth decreased to 14.3 GHz at 8 mA injection current due to heat generation inside the device. For the 7 μm oxide aperture VCSEL, as the injection current increases from 3 mA to 9 mA, the small signal modulation bandwidth increases from 14.1 GHz to the maximum 15.2 GHz, and then dropped to 13.1 GHz. Under

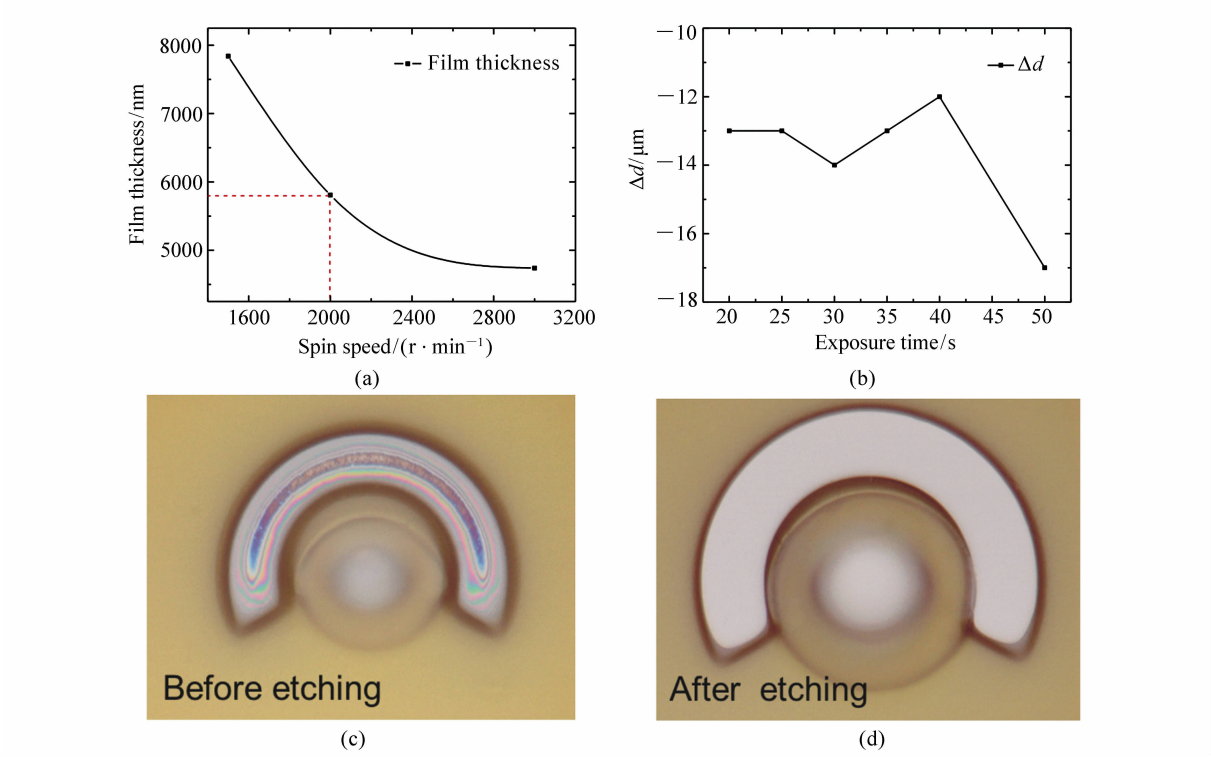

Fig. 3 (a) Relationship between spin speed and film thickness of BCB. (b) Difference in aperture diameter(Δd) between lithography and BCB patterns at various exposure times. (c) Top-view images of the thin BCB layer before dry etching and (d) after dry etching

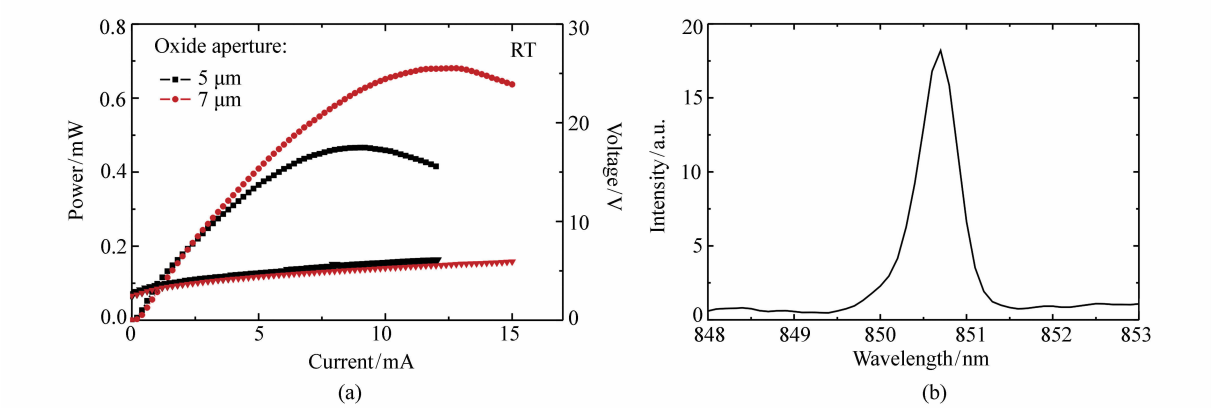

Fig. 4 (a) Static P-I-V characteristics of BCB-planarized VCSELs with a 5 μm and 7 μm oxide aperture at room temperature. (b) Electrical-luminescence spectrum for the VCSEL at room temperature and current injection of 10.0 mA

small injection current bias at 2 mA for 5 μm oxide aperture and 3 mA for 7 μm oxide aperture, the intensity modulation can follow the current modulation up to resonance frequency. An obvious enhancement of modulation response exists at the resonance. As shown in Fig. 5, beyond the resonance, the response dropped off dramatically. While, under the large injection currents, the responses measured in Fig. 5 are flat without peak frequency of resonance. The −3 dB modulation bandwidth increases with the resonance frequency until the damping becomes more and more strong. At same time, the −3 dB modulation bandwidth decreases with the further increase of resonance frequency and the damping.

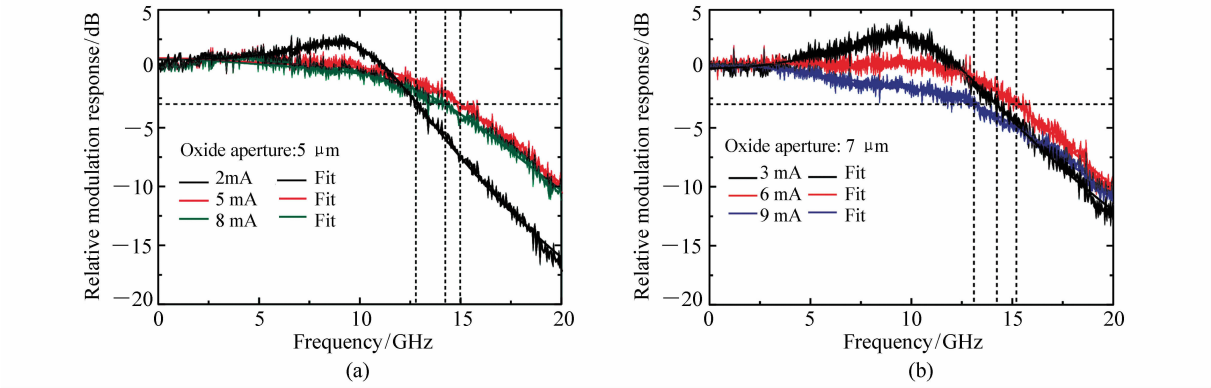

Fig. 5　Small-signal modulation response at room temperature at different bias currents for the BCB-planarized VCSEL with (a)5 μm and (b)7 μm oxide aperture

Fig. 6(a) plots the resonance frequency depending on the square value of injection current above the threshold current I_{th} for the VCSEL with oxide aperture of 5 μm and 7 μm. The data of resonance frequency is extracted from the fitting of the curves in Fig. 5 according to the transfer function[18]. As show in Fig. 6(a), resonance frequency f_r increases linearly with the low injection current. The slope, which is the rate of the resonance frequency increased with bias current, could be defined as D-factor of 8.746 GHz/mA$^{1/2}$ and 7.492 GHz/mA$^{1/2}$, for 5 μm and 7 μm oxide aperture VCSELs, respectively. The reason is that, under the same injection current, VCSEL with small oxide aperture has a smaller active region volume than that of lager oxide aperture.

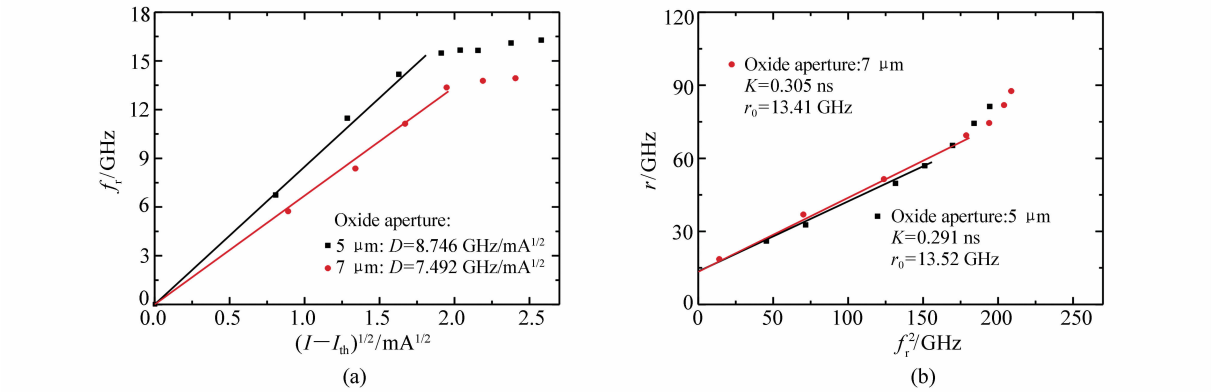

Fig. 6　(a) Plot of the resonance frequency for the VCSELs with 5 μm and 7 μm oxide aperture versus the square root of the current injection above the threshold current at room temperature. (b) Damping rate versus resonance frequency square for the VCSELs with 5 μm and 7 μm oxide aperture at room temperature

Fig. 6(b) plots the dependence of damping on the square of resonance frequency for the VCSELs with the oxide aperture of 5 μm and 7 μm, respectively. All the damping data are also extracted from the fitting results for the curves in Fig. 5. The damping increases in proportion to resonance frequency, which can be described as follows[19]

$$\gamma = Kf_r^2 + \gamma_0 \quad (1)$$

where K is the rate of the damping increased with the square of the resonance frequency, γ_0 is damping factor offset. As shown in Fig. 6(b), the damping increases linearly with f_r^2 at the beginning and then increases dramatically. The value of K-factor, which is determined by the photon lifetime, is 0.291 and

0.305 ns for the VCSELs with the 5 μm and 7 μm oxide apertures respectively, whose slight difference comes from the measurement errors and fabrication.

4 Conclusion

High-speed oxide confined 850 nm GaAs QWs VCSELs were designed and fabricated using a low-k BCB planarization technique. BCB has a very low dielectric constant of 2.65 and a 6 μm thick layer was deposited using a spin-coating process. The parasitic cutoff frequency of the VCSEL using BCB planarization technique increased from 10.6 GHz to 17.8 GHz compared with the SiO_2-passivated VCSEL at 7 μm oxide aperture. The small signal modulation bandwidth of the low-k BCB planarization VCSELs with 5 μm and 7 μm oxide aperture have been achieved to 15 GHz and 15.2 GHz, respectively, mainly limited by the damping and resonance frequency.

References:

[1] 海一娜,邹永刚,田锟,等. 水平腔面发射半导体激光器研究进展[J]. 中国光学,2017,10(2):194-206.
HAI Y N,ZOU Y G,TIAN K,*et al*. Research progress of horizontal cavity surface emitting semiconductor lasers[J]. *Chinese Optics*,2017,10(2):194-206.

[2] 黄海华,刘云,杨晔,等. 850 nm 锥形半导体激光器的温度特性[J]. 中国光学,2013,6(2):201-207.
HAI H H,LIU Y,YANG Y,*et al*. Temperature characteristics of 850 nm tapered semiconductor lasers[J]. *Chinese Optics*,2013,6(2):201-207.

[3] 咸晓东,叶淑娟,张楠,等. 面发射分布反馈半导体激光器及光栅耦合半导体激光器[J]. 中国光学,2010,3(5):415-431.
QI X D,YE SH J,ZHANG N,*et al*. Surface-emitting distributed-feedback semiconductor lasers and grating-coupled laser diodes[J]. *Chinese Optics*,2010,3(5):415-431.

[4] WESTBERGH P,GUSTAVSSON J S,HAGLUND A,*et al*.. High-speed, low-current-density 850 nm VCSELs[J]. *IEEE J. Sel. Topics Quantum Electron*.,2009,15(3):694-703.

[5] WESTBERGH P,GUSTAVSSON J S,KO? GEL B,*et al*.. Impact of photon lifetime on high-speed VCSEL performance [J]. *IEEE J. Sel. Topics Quantum Electron*.,2011,17(6):1603-1613.

[6] LARISCH G,MOSER P,LOTT J A,*et al*.. Impact of photon lifetime on the temperature stability of 50 Gb/s 980 nm VCSELs[J]. *IEEE Photon. Technol. Lett*.,2016,28(21):2327-2330.

[7] HAGLUND E,WESTBERGH P,GUSTAVSSON J S,*et al*.. High-speed VCSELs with strong confinement of optical fields and carriers[J]. *J. Lightwave Technol*.,2016,34(2):269-277.

[8] MOSER P,LOTT J A,BIMBERG D. Energy efficiency of directly modulated oxide-confined high bit rate 850-nm VCSELs for optical interconnects[J]. *IEEE J. Sel. Topics Quantum Electron*.,2013,19(4):1702212-1702212.

[9] WESTBERGH P,SAFAISINI R,HAGLUND E,*et al*.. High-speed oxide confined 850-nm VCSELs operating error-free at 40 Gb/s up to 85 ℃[J]. *IEEE Photon. Technol. Lett*.,2013,25(8):768-771.

[10] LUCOVSKY G,RAYNER JR G B. Microscopic model for enhanced dielectric constants in low concentration SiO_2-rich noncrystalline Zr and Hf silicate alloys[J]. *Appl. Phys. Lett*.,2000,77(18):2912-2914.

[11] OU Y,GUSTAVSSON J S,WESTBERGH P,*et al*.. Impedance characteristics and parasitic speed limitations of high-speed 850-nm VCSELs[J]. *IEEE Photon. Technol. Lett*.,2009,21(24):1840-1842.

[12] CHANG Y C,COLDREN L A. Efficient, high-data-rate, tapered oxide-aperture vertical-cavity surface-emitting lasers [J]. *IEEE J. Sel. Topics Quantum Electron*.,2009,15(3):704-715.

[13] LI H,LOTT J A,WOLF P,*et al*.. Temperature-dependent impedance characteristics of temperature-stable high-speed 980-nm VCSELs[J]. *IEEE Photon. Technol. Lett*.,2015,27(8):832-835.

[14] COLDREN L A,CORZINE S W,MASHANOVITCH M L. *Diode Lasers and Photonic Integrated Circuits*[M]. New Jersey,MD:John Wiley & Sons,2012.

[15] LI H, WOLF P, MOSER P, *et al.*. Impact of the quantum well gain-to-cavity etalon wavelength offset on the high temperature performance of high bit rate 980-nm VCSELs[J]. *IEEE J. Quantum Electron.*, 2014, 50(8): 613-621.

[16] MOSER P, LOTT J A, LARISCH G, *et al.*. Impact of the oxide-aperture diameter on the energy efficiency, bandwidth, and temperature stability of 980-nm VCSELs[J]. *J. Lightwave Technol.*, 2015, 33(4): 825-831.

[17] LARSSON A, WESTBERGH P, GUSTAVSSON J, *et al.*. High-speed VCSELs for short reach communication[J]. *Semicond. Sci. Technol.*, 2010, 26(1): 014017.

[18] HAGLUND E P, KUMARI S, WESTBERGH P, *et al.*. 20-Gb/s modulation of silicon-integrated short-wavelength hybrid-cavity VCSELs[J]. *IEEE Photon. Technol. Lett.*, 2016, 28(8): 856-859.

[19] HAGLUND E P, WESTBERGH P, GUSTAVSSON J S, *et al.*. Impact of damping on high-speed large signal VCSEL dynamics[J]. *J. Lightwave Technol*, 2015, 33(4): 795-801.

作者简介：

何晓颖(1981—)，女，湖北荆州人，博士，副教授，2009 年于华中科技大学获得博士学位，主要从事半导体激光器、光纤激光器、石墨烯光电子器件等新型光电子器件的研究工作。

郭　霞(1974—)，女，山东青岛人，博士，教授，1996 年于聊城大学获得学士学位，2003 年于北京工业大学获得博士学位，主要从事半导体激光器、发光二极管等光电子器件方面的研究。E-mail: guox@ bupt. edu. cn